AD-A047 415 NAVAL RESEARCH LAB WASHINGTON D C F/G 20/1
HORIZONTAL RAY CURVATURE EFFECTS IN BASINS, TROUGHS, AND NEAR S--ETC(U)
SEP 77 C H HARRISON

UNCLASSIFIED NRL-8144 SBIE-AD-E000 035 NL

1 OF 1
ADA047415

END
DATE FILMED
1-78
DDC

NRL Report 8144

Horizontal Ray Curvature Effects In Basins, Troughs, and Near Seamounts by Use of Ray Invariants

C. H. HARRISON

Admiralty Research Laboratory
Teddington, Middlesex, England

and

Applied Ocean Acoustics Branch
Acoustics Division

September 30, 1977

NAVAL RESEARCH LABORATORY
Washington, D.C.

SECURITY CLASSIFICATION OF THIS PAGE (When Data Entered)

REPORT DOCUMENTATION PAGE

READ INSTRUCTIONS BEFORE COMPLETING FORM

1. REPORT NUMBER: NRL [redacted] 8144
2. GOVT ACCESSION NO.
3. RECIPIENT'S CATALOG NUMBER

4. TITLE (and Subtitle): HORIZONTAL RAY CURVATURE EFFECTS IN BASINS, TROUGHS, AND NEAR SEAMOUNTS BY USE OF RAY INVARIANTS.

5. TYPE OF REPORT & PERIOD COVERED: Interim report on a continuing NRL Problem

6. PERFORMING ORG. REPORT NUMBER

7. AUTHOR(s): C. H. Harrison

8. CONTRACT OR GRANT NUMBER(s)

9. PERFORMING ORGANIZATION NAME AND ADDRESS
Naval Research Laboratory
Washington, D.C. 20375

10. PROGRAM ELEMENT, PROJECT, TASK AREA & WORK UNIT NUMBERS
NRL Problem 81S01-47
Project ZF52-552-01-62759N-
ASL 4-0002

11. CONTROLLING OFFICE NAME AND ADDRESS
Naval Material Command, Washington, D.C.
Naval Ocean Systems Center, San Diego, Calif.
(Arctic Submarine Laboratory)

12. REPORT DATE: September [redacted] 1977

13. NUMBER OF PAGES: 24

14. MONITORING AGENCY NAME & ADDRESS (if different from Controlling Office)

15. SECURITY CLASS. (of this report): UNCLASSIFIED

15a. DECLASSIFICATION/DOWNGRADING SCHEDULE

16. DISTRIBUTION STATEMENT (of this Report)
Approved for public release; distribution unlimited.

17. DISTRIBUTION STATEMENT (of the abstract entered in Block 20, if different from Report)

18. SUPPLEMENTARY NOTES

19. KEY WORDS (Continue on reverse side if necessary and identify by block number)

Acoustic propagation
Bottom reflection
Ray curvature, horizontal
Ray invariants
Ray tracing, analytical
Ray tracing, three-dimensional

20. ABSTRACT (Continue on reverse side if necessary and identify by block number)

Horizontal curvature of long-range underwater sound rays can be caused by repeated reflection from a sloping or undulating seabed. Ray invariants were used to derive analytical solutions for the horizontal projections of ray paths for many types of basins, troughs, and ridges. In an arbitrary basin (of low bottom slope) containing isovelocity water, the elevation angle of the ray depends only on the ratio of the basin depth at source and receiver and on the initial ray angle. In a basin with rotational symmetry or a trough with constant cross section, the heading of the ray may be determined anywhere

(Continued)

DD FORM 1 JAN 73 1473 EDITION OF 1 NOV 65 IS OBSOLETE
S/N 0102-014-6601

SECURITY CLASSIFICATION OF THIS PAGE (When Data Entered)

20. (Continued)

from the initial heading, the final heading, and the elevation angle. Rough figures are derived for the geometrical spreading loss and reflection loss at the edge of a basin.

CONTENTS

HORIZONTAL RAY CURVATURE EFFECTS IN BASINS, TROUGHS, AND NEAR SEAMOUNTS BY USE OF RAY INVARIANTS

INTRODUCTION

Long-range underwater sound propagation is often influenced by regions of repeated surface and bottom reflection. Under these conditions, a component of bottom slope consistently to one side of the ray path may cause considerable horizontal curvature. For instance, it is easily shown (by considering source images) that the horizontal projection of the ray path above a plane sloping bottom is a hyperbola. Similarly, in a basin, one might expect to find ray paths that loop around the center to form a rosette-like shape. It is important to note that the curvature effect applies to rays of small as well as large grazing angles. Despite the larger number of reflections required at low grazing angles to produce a given change in heading, the consequent reduction in reflection coefficient may allow propagation losses that are not prohibitively large. This phenomenon was first dealt with by Weston [1,2], and some of the effects in the vertical plane were investigated later by Milder [3].

Field recordings of remote, powerful pulsed sources (sometimes the equivalent of a ton or more of explosives) [4-10] often contain discrete and continuous arrivals stretching over periods on the order of 10 min, depending on the size of the basin. This type of echo is often interpreted in a phenomenological way as a single reflection or scatter from one or more seamounts or basin walls [4-6]. Whether the ray deflection is really caused by multiple surface and bottom reflections or by a single scatter remains to be proved, but whatever the cause, as long as the seabed is not horizontal, after bottom interaction the ray path cannot be considered to remain in the same vertical plane.

This report attempts to find a detailed theoretical explanation for the long ray paths encountered in basins by using ray invariants to calculate the horizontal projection of the multiply-reflected ray. The treatment differs from that of Weston [1,2] in choosing, as a starting point, a simpler sound velocity structure, but more complex bottom topography.

I. THREE-DIMENSIONAL RAY PATHS

To construct a three-dimensional ray path, it is first necessary to calculate the change in ray angle after a single reflection.

Figure 1 shows a ray striking a bottom that is assumed to slope down at angle γ in the y direction; θ, ϕ are incident ray elevation and azimuth angles with a prime added for reflected rays; and Φ is the local angle of incidence. We wish to find expressions for θ' and ϕ' in terms of the other variables, and these may be shown, by straightforward spherical trigonometry, to be

Manuscript submitted June 9, 1977.

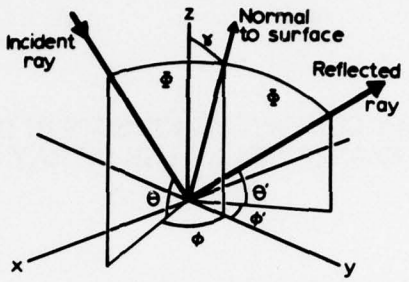

Fig. 1 — The geometry for a single reflection

$$\sin\theta' = \cos 2\gamma \sin\theta + \sin 2\gamma \cos\theta \cos\phi \tag{1}$$

and

$$\tan\phi' = \frac{\sin\phi \cos\theta}{(\sin\theta \sin 2\gamma - \cos\theta \cos 2\gamma \cos\phi)} \tag{2}$$

The change in heading of the ray after reflection α, (where $\alpha = \pi - \phi - \phi'$) is given from Eq. (2) by

$$\tan\alpha = \frac{\tan\phi (\sin\theta \sin 2\gamma - \cos 2\gamma \cos\theta \cos\phi) + \sin\phi \cos\theta}{\tan\phi (\sin\phi \cos\theta + \cos 2\gamma \cos\theta \cos\phi) - \sin\theta \sin 2\gamma} \tag{3}$$

and this, as expected, is zero if the bottom slope γ is zero. Another useful equation that is independent of γ may be derived from Fig. 1, and this is

$$\cos\theta' \sin\phi' = \cos\theta \sin\phi. \tag{4}$$

Consider, now, a ray in a uniform medium bounded by a plane upper surface and a bottom of arbitrary form but low slopes. At the ith bottom reflecting point we denote local slope, incident elevation and azimuth angles by γ_i, θ_i, and ϕ_i, respectively. Since the upper surface is horizontal, the elevation angle of the ray *reflected* from the ith point θ_i' is the same as the elevation of the *incident* ray at the $(i + 1)$th point θ_{i+1}; however, a similar relation is not generally true for the azimuth angles ϕ_i' and ϕ_{i+1} because the direction of bottom slope may change from point to point (Fig. 2). After the first reflection, we have from Eq. (1)

$$\sin\theta_1 = \sin\theta_0 + 2\gamma_0 \cos\theta_0 \cos\phi_0, \tag{5}$$

which for later convenience we write as

$$\sin\theta_1 = \sin\theta_0 (1 + 2\gamma_0 \cot\theta_0 \cos\phi_0). \tag{6}$$

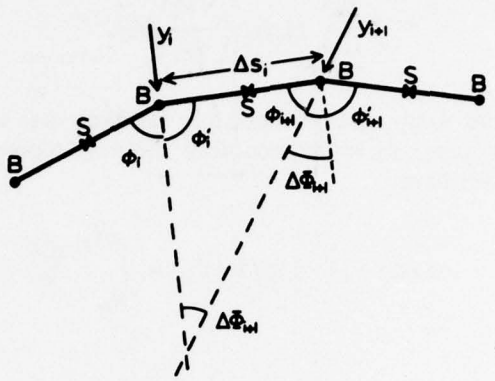

Fig. 2 — Horizontal projection of a ray path showing bottom reflection points *B*, surface reflection points *S*, and the changes in bottom slope directions *y* in between

After the nth reflection, repeated use of Eq. (6) gives

$$\sin \theta_n = \sin \theta_0 \prod_{i=0}^{n-1} (1 + 2\gamma_i \cot \theta_i \cos \phi_i). \tag{7}$$

Taking logarithms of both sides yields

$$\log (\sin \theta_n) = \log (\sin \theta_0) + \sum_{i=0}^{n-1} \log (1 + 2\gamma_i \cot \theta_i \cos \phi_i). \tag{8}$$

Provided $2\gamma_i \cot \theta_i \cos \phi_i$ is much less than unity, the term $\log (1 + 2\gamma_i \cot \theta_i \cos \phi_i)$ may be replaced by $2\gamma_i \cot \theta_i \cos \phi_i$. For this to be true, the rays must not be too close to the horizontal, although this restriction is not severe since γ_i is already very small. Roughly speaking, ray elevation angles must be greater than twice the local bottom slope so that rays cannot be reflected downward from the bottom. Equation (8) is now

$$\log (\sin \theta_n) = \log (\sin \theta_0) + \sum_{i=0}^{n-1} 2\gamma_i \cot \theta_i \cos \phi_i, \tag{9}$$

and the summation may be expanded in terms of the water depth. The horizontal spacing between bottom reflections (Fig. 2) is $\Delta s_i = 2H_i \cot \theta_i$, and the component of Δs_i in local downslope direction y_i is

$$\Delta y_i = \Delta s_i \cos \phi_i = 2H_i \cot \theta_i \cos \phi_i. \tag{10}$$

Now, since $\gamma_i = - dH_i/dy_i$, the summation in Eq. (9) may be replaced by

$$\sum_{i=0}^{n-1} (1/H_i)\left(\frac{dH_i}{dy_i}\right)\Delta y_i$$

and, provided the bottom slope changes smoothly between one reflection point and the next so that the term in brackets varies smoothly, we may replace the summation sign by an integral sign. Then we have

$$\log (\sin \theta_n) = \log (\sin \theta_0) - \int_{H_0}^{H_n} \frac{dH}{H} , \tag{11}$$

which leads to

$$\sin \theta_n = \sin \theta_0 \frac{H_0}{H_n} . \tag{12}$$

Thus $H \sin \theta$ is invariant for a particular ray, and this is a special case of Weston's invariant [1]

$$\int_0^H (\sin \theta / c)\, dz.$$

For a given initial elevation angle θ_0, the elevation angle at another site depends only on the ratio of the water depths at that site and at the source (regardless of the coordinate system or functional form at the seabed). On a map of bottom topography, contours of water depth are also contours of ray elevation angle.

This result could have been derived much more directly from Eq. (1) except that the approximation used between Eqs. (8) and (9) would not have appeared so clearly. Another result may be derived from Eq. (4); however, this time the validity does not depend on small bottom slopes although a usable form depends on the shape of the bottom.

Using Eq. (4) repeatedly for a trough of arbitrary but constant cross section, so that the y_i axes all point in the same direction and $\theta_i' = \theta_{i+1}$ and $\phi_i' = \pi - \phi_{i+1}$, we have

$$\cos \theta_{i+1} \sin \phi_{i+1} = \cos \theta_i \sin \phi_i; \tag{13}$$

and, after n reflections,

$$\cos \theta_n \sin \phi_n = \cos \theta_0 \sin \phi_0. \tag{14}$$

Thus for a trough of fixed cross section, $\cos \theta \sin \phi$ is invariant.

For the more general case, as in Fig. 2, where maximum bottom slope direction y_i is a function of position, we have $\theta_i' = \theta_{i+1}$ and $\phi_i' = \pi - \phi_{i+1} - \Delta\Phi_{i+1}$, where $\Delta\Phi_{i+1}$ is the change in maximum bottom slope direction encountered between the ith and $(i + 1)$th bottom reflection (assumed to be a small angle).

At the ith reflection,

$$\cos \theta_i' \sin \phi_i' = \cos \theta_i \sin \phi_i; \tag{15}$$

and at the $(i + 1)$th reflection,

$$\cos \theta_{i+1}' \sin \phi_{i+1}' = \cos \theta_{i+1} \sin (\pi - \phi_{i+1} - \Delta\Phi_{i+1}) = \cos \theta_{i+1} \sin \phi_{i+1}(1 + \cot \phi_{i+1}\, \Delta\Phi_{i+1}). \tag{16}$$

Using Eq. (16) repeatedly and taking logarithms of both sides results in

$$\log (\cos \theta_n' \sin \phi_n') = \log (\cos \theta_0 \sin \phi_0) + \sum_{i=0}^{n} \log (1 + \cot \phi_i\, \Delta\Phi_i). \tag{17}$$

In the last term, $\cot \phi_i$ may be written as $(\Delta y_i/\Delta x_i)$, where Δy_i and Δx_i are the y and x components of the distances between the ith and $(i - 1)$th reflection point. Provided the ray is not close to the intersection of the y_i and y_{i+1} axes, which is the local center of curvature of the depth contours, $\Delta\Phi_i/\Delta x_i$ is a good approximation for the contour curvature, and the last term in the summation is much less than unity. If we use the small argument approximation for $\log (1 + X)$, we have

$$\log (\cos \theta_n' \sin \phi_n') = \log (\cos \theta_0 \sin \phi_0) + \sum_{i=0}^{n} \frac{1}{\rho}\, \Delta y_i, \tag{18}$$

where ρ is the local radius of curvature of the depth contours.

If the curvature of the depth contours changes smoothly from reflection point to reflection point, the summation sign can be replaced by an integral sign:

$$\log (\cos \theta_n' \sin \phi_n') = \log (\cos \theta_0 \sin \phi_0) + \int \frac{dy}{\rho}\ . \tag{19}$$

If the change in position of the center of curvature is always much smaller than Δy_i, then dy may be replaced by $-d\rho$ and integration performed to give

$$\cos \theta_n' \sin \phi_n' \rho_n = \cos \theta_0 \sin \phi_0 \rho_0. \tag{20}$$

However, this last condition is somewhat restrictive, and the only type of basin for which Eq. (20) is unconditionally true is that with either parallel, straight depth contours or concentric, circular contours. The former case corresponds to a trough of arbitrary cross section and has already been considered. The latter corresponds to a basin with rotational symmetry where ρ_0, ρ_n are now the polar coordinates of source and receiver, respectively, r_0, r_n measured from the center of the basin:

$$\cos\theta_n' \sin\phi_n' r_n = \cos\theta_0 \sin\phi_0 r_0. \tag{21}$$

Thus for a circular basin, $r \cos\theta \sin\phi$ is invariant.

For a basin of any other shape, there are two alternatives: use Eq. (19) in an iterative fashion since the integral contains dy which depends on ray path, or divide the whole area into portions of circular basins or straight troughs, each with its own separate, invariant, matching ray angles at the boundaries.

Combining Eq. (12) and either Eq. (14) or (21), we can find a relation for azimuth angle ϕ_n with a view to calculating a continuous curve representing the horizontal projection of the ray path. After many surface and bottom reflections, the difference between θ_n, ϕ_n and θ_n', ϕ_n' becomes insignificant; so, dropping the subscripts n and primes, we have for the trough case

$$\sin\phi = \sin\phi_0 \cos\theta_0 H/(H^2 - H_0^2 \sin^2\theta_0)^{1/2}. \tag{22}$$

The distance traveled along the trough is given by

$$x = \int dx = \int dy \tan\phi = \int \frac{\sin\phi_0 \cos\theta_0 \, dy}{\left[(1 - \sin^2\phi_0 \cos^2\theta_0) - \dfrac{H_0^2}{H^2} \sin^2\theta_0\right]^{1/2}}. \tag{23}$$

Given the cross section of the trough $H(y)$, this integral can be performed, and the ray path $y(x)$ is then known. Some examples are given in the next section. Note that the trough can be turned into a ridge simply by making $H(y)$ an increasing, rather than decreasing, function of y.

The total ray length is given by

$$s = \int ds = \int dy \sec\theta \sec\phi = \int \frac{\tan\phi \, dy}{\cos\theta_0 \sin\phi_0} = \frac{x}{\sin\phi_0 \cos\theta_0}, \tag{24}$$

and the rather surprising result is that *the ray length is always proportional to the component of distance traveled along the trough.*

For the circular basin (or seamount), Eq. (22) is replaced by

$$\sin\phi = \sin\phi_0 \cos\theta_0 H \frac{r_0}{r} /(H^2 - H_0^2 \sin^2\theta_0)^{1/2}, \tag{25}$$

and the ray path in polar coordinates r, Φ is derived from

$$\Phi = \int d\Phi = \int \frac{dr}{r} \tan\phi = \int \frac{\sin\phi_0 \cos\theta_0 \, dr}{r\left[\frac{r^2}{r_0^2}\left(1 - \frac{H_0^2}{H^2}\sin^2\theta_0\right) - \sin^2\phi_0 \cos^2\theta_0\right]^{1/2}} . \tag{26}$$

The total ray length is given by

$$s = \int ds = \int dr \sec\theta \sec\phi = \int \frac{\tan\phi \, r dr}{\sin\phi_0 \cos\theta_0 \, r_0} = \frac{\int r^2 d\Phi}{r_0 \sin\phi_0 \cos\theta_0}$$

$$= \frac{2 \text{ (area of trajectory swept out)}}{r_0 \sin\phi_0 \cos\theta_0} . \tag{27}$$

The ray length in a basin is always proportional to the area swept out by the radial coordinate of the ray as it moves around the basin.

II. EXAMPLES OF HORIZONTAL RAY PATH PROJECTIONS FOR TROUGHS AND RIDGES

A. Troughs

Note that only the shape of the trough need be specified; the absolute depth is not needed. In all cases the characteristic width of the trough is R.

(i) $H(y) \propto [1 + (y^2/R^2)]^{-1/2}$

$$x = \int \frac{(R^2 + y_0^2)^{1/2} \cot\theta_0 \sin\phi_0 \, dy}{(\cot^2\theta_0 \cos^2\phi_0 \, (R^2 + y_0^2) + y_0^2 - y^2)^{1/2}}$$

$$y = (\cot^2\theta_0 \cos^2\phi_0 \, (R^2 + y_0^2) + y_0^2)^{1/2} \sin\left[\frac{x + x'}{(R^2 + y_0^2)^{1/2} \cot\theta_0 \sin\phi_0}\right], \tag{28}$$

where x' is a constant given by

$$\sin\left[\frac{x'}{(R^2 + y^2)^{1/2} \cot\theta_0 \sin\phi_0}\right] = \frac{y_0}{[\cot^2\theta_0 \cos^2\phi_0 \, (R^2 + y_0^2) + y_0^2]^{1/2}} . \tag{29}$$

So the rays are sine waves of wavelength $2\pi(R^2 + y_0^2)^{1/2} \cot\theta_0 \sin\phi_0$ and amplitude $[(R^2 + y_0^2) \cot^2\theta_0 \cos^2\phi_0 + y_0^2]^{1/2}$.

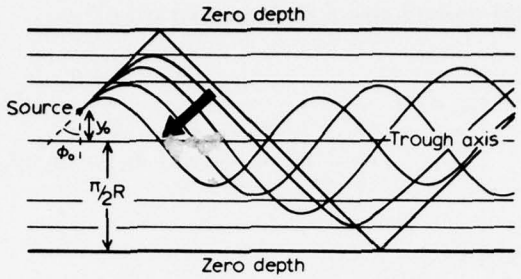

Fig. 3 — Horizontal projection of ray paths for a trough of cosine cross section $H(y) \propto \cos(y/R)$, for constant ϕ_0, and θ_0 increasing from zero (indicated by a broad arrow)

(ii) $H(y) \propto \cos(y/R)$ (cosine trough)

$$x = \frac{\sin\phi_0 \cot\theta_0 \cos(y/R)\, dy}{\{[1 - \sin^2\phi_0 \cos^2\theta_0 - \sin^2\theta_0 \cos^2(y_0/R)] - (1 - \sin^2\phi_0 \cos^2\theta_0)\sin^2(y/R)\}^{1/2}}$$

$$\sin(y/R) = \left(1 - \frac{\cos^2(y_0/R)\sin^2\theta_0}{(1 - \sin^2\phi_0 \cos^2\theta_0)}\right)^{1/2} \sin\left[\frac{(x + x')(1 - \sin^2\phi_0 \cos^2\theta_0)}{R \sin\phi_0 \cos\theta_0}\right], \tag{30}$$

where x' is given by

$$\sin\left[\frac{x'(1 - \sin^2\phi_0 \cos^2\theta_0)}{R \sin\phi_0 \cos\theta_0}\right] = \frac{\sin(y_0/R)}{\left(1 - \frac{\cos^2(y_0/R)\sin^2\theta_0}{(1 - \sin^2\phi_0 \cos^2\theta_0)}\right)^{1/2}}. \tag{31}$$

When the first term on the right of Eq. (30) is set to 1 by, for instance, making $y_0 = \pi R/2$, which corresponds to putting the source at the edge of the trough, the ray path is a periodic zigzag line from one side of the trough to the other as in Fig. 3. When the same term is made small compared with unity by making y_0/R small and θ_0 or ϕ_0 large, the ray path is a sine wave of wavelength

$$2\pi R \frac{\sin\phi_0 \cot\theta_0}{(1 - \sin^2\phi_0 \cos^2\theta_0)}$$

and amplitude

$$R\left(1 - \frac{\cos^2(y_0/R)\sin^2\theta_0}{(1 - \sin^2\phi_0 \cos^2\theta_0)}\right)^{1/2}.$$

(iii) $H(y) \propto [1 - (y^2/R^2)]^{1/2}$ *(elliptical trough)*

(Note that the small bottom slope approximation may be violated near the edges.)

$$x = \int \frac{\sin \phi_0 \cot \theta_0 \, (R^2 - y^2)^{1/2} \, dy}{(\cot^2 \theta_0 \cos^2 \phi_0 \, R^2 + y_0^2 - y^2)^{1/2}}$$

$$x + x' = R \sin \phi_0 \cot \theta_0 \, E[k, \sin^{-1} (y/kR)], \tag{32}$$

where

$$x' = R \sin \phi_0 \cot \theta_0 \, E[k, \sin^{-1} (y/kR)], \tag{33}$$

and

$$k = [\cot^2 \theta_0 \cos^2 \phi_0 + (y_0^2/R^2)]^{1/2}, \tag{34}$$

where $E(k, \alpha)$ is an elliptic integral of the second kind

$$E(k, \alpha) = \int_0^{\alpha} (1 - k^2 \sin^2 \theta)^{1/2} \, d\theta.$$

y is still always periodic in x, and again for small k; that is, y_0/R small and θ_0 large or ϕ_0 close to $\pi/2$, $E(k, \alpha) = \alpha$, and the ray path is a sine wave of wavelength $2\pi R \sin \phi_0 \cot \theta_0$ and amplitude $Rk = (R^2 \cot^2 \theta_0 \cos^2 \phi_0 + y_0^2)^{1/2}$.

B. Ridges

(i) $H(y) \propto [1 - (y^2/R^2)]^{-1/2}$ *(for* $|y| < R$ *and* $|y_0| < R$*)*

$$x = \int \frac{(R^2 - y_0^2)^{1/2} \cot \theta_0 \sin \phi_0 \, dy}{[\cot^2 \theta_0 \cos^2 \phi_0 \, (R^2 - y_0^2) - y_0^2 + y^2]^{1/2}} \, .$$

For

$$|y_0| < \frac{R \cot \theta_0 \cos \phi_0}{(1 + \cot^2 \theta_0 \cos^2 \phi_0)^{1/2}} \, ,$$

$$y = (\cot^2 \theta_0 \cos \phi_0 \, (R^2 - y_0^2) - y_0^2)^{1/2} \sinh \left[\frac{x + x'}{(R^2 - y_0^2)^{1/2} \cot \theta_0 \sin \phi_0} \right], \tag{35}$$

and, for

$$R > |y_0| > \frac{R \cot\theta_0 \cos\phi_0}{(1 + \cot^2\theta_0 \cos^2\phi_0)^{1/2}} ,$$

$$y = (y_0^2 - \cot^2\theta_0 \cos^2\phi_0 (R^2 - y_0^2))^{1/2} \cosh\left[\frac{x + x'}{(R^2 - y_0^2)^{1/2} \cot\theta_0 \sin\phi_0}\right] \quad (36)$$

with x' given by putting $x = 0$ with $y = y_0$. These curves are shown in Fig. 4. The cosh and sinh families represent rays that are deflected away from the ridge to either side.

(ii) $H(y) \propto \cosh(y/R)$

$$x = \int \frac{\sin\phi_0 \cot\theta_0 \cosh(y/R)\, dy}{\{[1 - \sin^2\phi_0 \cos^2\theta_0 - \sin^2\theta_0 \cosh^2(y_0/R)] + (1 - \sin^2\phi_0 \cos^2\theta_0) \sinh^2(y/R)\}^{1/2}} .$$

For $\cosh(y_0/R) < (\operatorname{cosec}^2\theta_0 - \sin^2\phi_0 \cot^2\theta_0)^{1/2}$,

$$\sinh(y/R) = \left(1 - \frac{\cosh^2(y_0/R)}{\operatorname{cosec}^2\theta_0 - \sin^2\phi_0 \cot^2\theta_0}\right)^{1/2} \sinh\left[\frac{(x + x')(1 - \sin^2\phi_0 \cos^2\theta_0)}{R \sin\phi_0 \cos\theta_0}\right] \quad (37)$$

and, for $\cosh(y_0/R) > (\operatorname{cosec}^2\theta_0 - \sin^2\phi_0 \cot^2\theta_0)^{1/2}$,

$$\cosh(y/R) = \left(\frac{\cosh^2(y_0/R)}{\operatorname{cosec}^2\theta_0 - \sin^2\phi_0 \cot^2\theta_0} - 1\right)^{1/2} \cosh\left[\frac{(x + x')(1 - \sin^2\phi_0 \cos^2\theta_0)}{R \sin\phi_0 \cos\theta_0}\right] . \quad (38)$$

These curves are qualitatively similar to those of the last example.

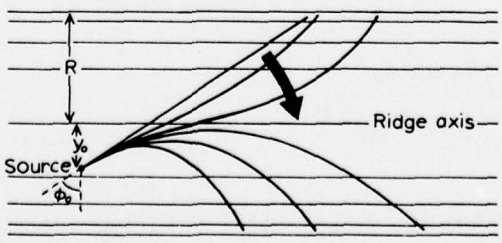

Fig. 4 — Horizontal projection of ray paths for a ridge of cross section $H(y) \propto [1 - (y^2/R^2)]^{-1/2}$, for constant ϕ_0, and θ_0 increasing from zero (indicated by a broad arrow)

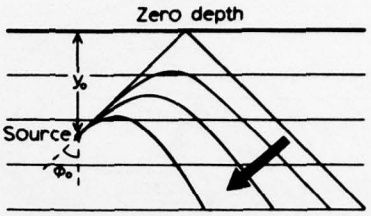

Fig. 5 — Horizontal projection of ray paths for tilted-plane seabed $H(y) \propto y$, for constant ϕ_0, and θ_0 increasing from zero (indicated by a broad arrow)

(iii) $H(y) \propto y$ *(wedge)*

$$x = \int \frac{\sin\phi_0 \cot\theta_0 \, y \, dy}{[(\operatorname{cosec}^2\theta_0 - \cot^2\theta_0 \sin^2\phi_0)\, y^2 - y_0^2]^{1/2}}$$

$$y^2 (1 - \cos^2\theta_0 \sin^2\phi_0) = \left(\frac{x\,(1 - \cos^2\theta_0 \sin^2\phi_0)}{\sin\phi_0 \cos\theta_0} - y_0 \cos\theta_0 \cos\phi_0 \right)^2 + y_0^2 \sin^2\theta_0 . \tag{39}$$

The ray path is a hyperbola as shown in Fig. 5. This result will be used later in the intensity estimation.

III. EXAMPLES OF HORIZONTAL RAY PATH PROJECTIONS FOR A BASIN AND A SEAMOUNT

A. Basin

(i) $H(r) \propto [1 + (r^2/R^2)]^{-1/2}$ *(a rotation of the first trough cross section)*

$$\Phi = \int \frac{r_0 (R^2 + r_0^2)^{1/2} \cot\theta_0 \sin\phi_0 \, dX}{2X\{-X^2 + [(R^2 + r_0^2)\operatorname{cosec}^2\theta_0 - R^2]X - \cot^2\theta_0 \sin^2\phi_0 \, r_0^2 (R^2 + r_0^2)\}^{1/2}} ,$$

where $X = r^2$ and r_0 is the radial coordinate of the source.

The solution of this integral is

$$\sin[2(\Phi + \Phi')] = \frac{A - B/r^2}{(A^2 - 2B)^{1/2}} , \tag{40}$$

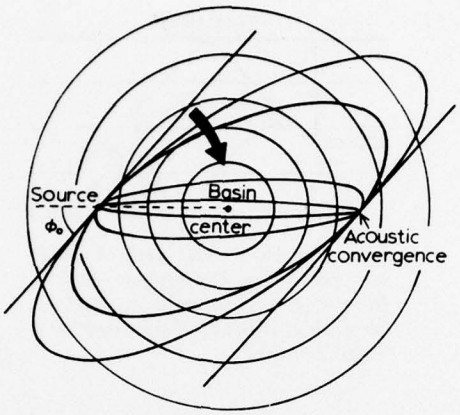

Fig. 6 — Horizontal projection of ray paths for a circular basin of cross section $H(r) \propto [1 + (r^2/R^2)]^{-1/2}$, for constant ϕ_0, and θ_0 increasing from zero (indicated by a broad arrow)

where Φ' is a constant given by

$$\sin [2\Phi'] = \frac{A - B/r_0^2}{(A^2 - 2B)^{1/2}} , \tag{41}$$

where

$$A = (R^2 + r_0^2) \operatorname{cosec}^2 \theta_0 - R^2$$

$$B = 2 \cot^2 \theta_0 \sin^2 \phi_0 \, r_0^2 (R^2 + r_0^2).$$

The ray path is an ellipse centered about the center of the basin (Fig. 6). One might have expected a rosette; however, for this particular type of basin, the ray covers the same path again after one revolution.

An ellipse is given in terms of its minor and major axes a, b, respectively, by

$$\frac{x^2}{a^2} + \frac{y^2}{b^2} = 1 \text{ or } \cos 2\Phi = - \frac{(a^2 + b^2) + 2 a^2 b^2 / r^2}{b^2 - a^2} ,$$

where

$$a^2 = (B/A)/[(1 - 2B/A^2)^{1/2} + 1]$$

$$b^2 = (B/A)/[1 - (1 - 2B/A^2)^{1/2}].$$

Note that all ray paths converge on a point diametrically opposite the source regardless of their initial heading or elevation angle (ϕ_0, θ_0).

The ray length for the ellipse (which is not an elliptic integral because of the up-and-down motion of the ray) is given in terms of r by

$$\sin\left[\frac{2r_0 \sin\phi_0 \cos\theta_0 (s+s')}{(B/2)^{1/2}}\right] = \frac{2r^2 - A}{(A^2 - 2B)^{1/2}}, \tag{42}$$

or, alternatively in terms of Φ, by

$$\tan\left[\frac{r_0 \sin\phi_0 \cos\theta_0 (s+s'')}{(B/2)^{1/2}}\right] = \frac{A \tan(\Phi + \Phi') - (A^2 - 2B)^{1/2}}{(2B)^{1/2}}, \tag{43}$$

where s', s'' are given by substituting $s = 0$ with either $r = r_0$ or $\Phi = \Phi_0$. For a whole circuit of the basin, the ray length is given from Eq. (42) or (43) by

$$s_c = 2\pi(R^2 + r_0^2)^{1/2} \operatorname{cosec}\theta_0. \tag{44}$$

This could also have been derived by substituting πab in Eq. (27) for the area of ellipse swept out.

B. Seamount

(i) $H(r) \propto r$ (conical seamount: apex at the sea surface)

$$\Phi = \int \frac{r_0 \sin\phi_0 \cos\theta_0 \, dr}{r[r^2 - r_0^2(1 - \cos^2\theta_0 \cos^2\phi_0)]^{1/2}}$$

$$r = r_0(1 - \cos^2\theta_0 \cos^2\phi_0)^{1/2} \operatorname{cosec}\left[\frac{(1 - \cos^2\theta_0 \cos^2\phi_0)^{1/2}}{\sin\phi_0 \cos\theta_0} (\Phi + \Phi')\right] \tag{45}$$

Here, Φ' is given by putting $\Phi = 0$ and $r = r_0$. These ray paths are shown in Fig. 7.

IV. THE EFFECT OF REFRACTION ON THE RAY PATHS

Up till now, we have assumed the sound velocity to be constant so that surface-to-bottom ray segments are straight lines. This is probably not too bad an approximation in regions where there is surface and bottom reflection because the ray angles have to be comparatively steep, making ray curvature in the vertical plane less significant. It is possible to take refraction into account to see how good the approximation is.

Equations (1) and (4) for single reflection are still true provided the angles are measured at the seabed. Note that the invariant

$$\int_0^H \left(\frac{\sin\theta}{c}\right) dz$$

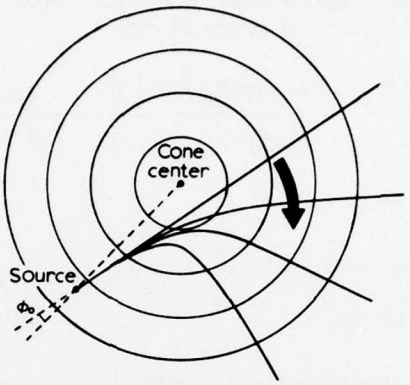

Fig. 7 — Horizontal projection of ray paths for a conical seamount $H(r) \propto r$, for constant ϕ_0, and θ_0 increasing from zero (indicated by a broad arrow)

derived by Weston [1] is also valid, but it governs the integral of elevation angle over depth as opposed to the elevation angle at the seabed. The first alteration comes after Eq. (9), where the spacing of adjacent reflection points Δs_i is now given (with z axis downwards) by

$$\Delta s_i = 2 \int_0^{H_i} \frac{c(z) \cos \theta_i \, dz}{(c_i^2 - c^2(z) \cos^2 \theta_i)^{1/2}} , \tag{46}$$

where c_i and θ_i are sound velocity and incident angle of the ith reflecting point on the bottom.

The equivalent of Eq. (6) for the change in elevation angle at the ith reflection point is

$$\sin \theta_i' = \sin \theta_i \left(1 - \frac{\Delta H_i \cot \theta_i}{\displaystyle\int_0^{H_i} \frac{c \cos \theta_i \, dz}{(c_i^2 - c^2 \cos^2 \theta_i)^{1/2}}} \right) , \tag{47}$$

but now the reflected angle at the $(i - 1)$th point is related to the incident angle at the ith point by Snell's law:

$$\cos \theta_i = \cos \theta_{i-1}' \left(\frac{c_i}{c_{i-1}} \right) . \tag{48}$$

The total change in angle after refraction and a single reflection is then

$$\sin^2 \theta_i' = \left[\left(\frac{c_i}{c_{i-1}}\right)^2 \sin^2 \theta_{i-1}' + \left(1 - \left(\frac{c_i}{c_{i-1}}\right)^2\right)\right]\left(1 - \frac{\Delta H_i \cot \theta_i}{\int_0^{H_i} \frac{c \cos \theta_i \, dz}{(c_i^2 - c^2 \cos^2 \theta_i)^{1/2}}}\right) . \quad (49)$$

After n reflections, we have

$$\sin^2 \theta_n' = \sin^2 \theta_0' \left(\frac{c_n}{c_0}\right)^2 \prod_{i=1}^{n} \left(1 - \frac{\Delta H_i \cot \theta_i}{\Delta s_i}\right)^2$$

$$+ \sum_{i=1}^{n} \left(\frac{c_n}{c_i}\right)^2 \left[1 - \left(\frac{c_i}{c_{i-1}}\right)^2\right] \prod_{j=i}^{n} \left(1 - \frac{\Delta H_j \cot \theta_j}{\Delta s_j}\right)^2 . \quad (50)$$

Since the variations in sound speed c are always amall, we may write $c = c_{00} + \delta(z)$, and Eq. (46) becomes

$$\Delta s_i \tan \theta_i = \frac{2c_{00}}{c_i} \int_0^{H_i} \frac{(1 + \delta/c_{00}) \, dz}{\{1 - [(c_{00} + \delta)^2 - c_i^2] \cot^2 \theta_i / c_i^2\}^{1/2}} . \quad (51)$$

Now, we may eliminate θ_i from the correction term in the denominator by using the uniform velocity invariant (Eq. (12)):

$$\Delta s_i \tan \theta_i = \frac{2c_{00}}{c_i} \int_0^{H_i} \frac{(1 + \delta/c_{00}) \, dz}{\{1 - [(c_{00} + \delta)^2 - c_i^2] \, (\mathrm{cosec}^2 \, \theta_0 \, H_i^2/H_0^2 - 1)/c_i^2\}^{1/2}} . \quad (52)$$

For a given velocity profile, $\Delta s_i \tan \theta_i$ is simply a function of H_i, H_0, and θ_0, and so we can substitute $\Delta s_i \tan \theta_i$ into Eq. (50) and evaluate the products as we did in the earlier section (assuming that $2\Delta H_i \cot \theta_i / \Delta s_i$ is always small):

$$\sin^2 \theta_n' = \sin^2 \theta_0' \left(\frac{c_n}{c_0}\right)^2 \exp[-2(F_n - F_0)]$$

$$+ c_n^2 \sum_{i=1}^{n} \left(\frac{1}{c_i^2} - \frac{1}{c_{i-1}^2}\right) \exp[-2(F_n - F_i)] , \quad (53)$$

where

$$F_n - F_0 = \int_{H_0}^{H_n} \frac{2dH}{\Delta s \tan \theta} .$$

The summation of Eq. (53) may be evaluated by rearranging its terms to give

$$1 - \left(\frac{c_n}{c_0}\right)^2 e^{-2(F_n - F_i)} + c_n^2 e^{-2F_n} \sum_{i=1}^{n-1} \frac{1}{c_i^2}\left(e^{2F_i} - e^{2F_{i+1}}\right).$$

Since the variations in c_i are always small, c_i may be taken out of this summation and Eq. (53) becomes

$$\sin^2 \theta_n' = \sin^2 \theta_0' \left(\frac{c_n}{c_0}\right)^2 e^{-2(F_n - F_0)} + \left\{(1 - \alpha) - \left[\left(\frac{c_n}{c_0}\right)^2 - \alpha\right] e^{-2(F_n - F_0)}\right\}, \tag{54}$$

where α is a number very close to unity (of order c_n/c_i) so that the second term in Eq. (54) makes only a small correction and the uncertainty in α has no significant effect. Equation (54) shows that, again, the elevation angle at any bottom point is known for a given initial angle and water depth. Despite the more complicated nature of this equation, contours of water depth on a map of bottom topography are still contours of ray elevation angle.

As an example, a linear velocity profile $\delta = [(z/H_0) - 1]\ \Delta c$ gives (assuming ray angles are not too close to the horizontal)

$$\sin \theta_n' = \sin \theta_0' \frac{H_0}{H}\left[1 - \frac{\Delta c}{c_{00}} \operatorname{cosec}^2 \theta_0 \left(\frac{\frac{H^3}{H_0^3} - 1}{6} - \frac{\frac{H^2}{H_0^2} - 1}{2}\right)\right] \tag{55}$$

A positive velocity gradient (velocity increasing downwards) results in a reduced spacing of reflection points for a given ray elevation angle at the seabed, so a ray traveling from deep to shallow water, for instance, would arrive at a given elevation angle sooner (in deeper water) than it would if it had traveled through water of uniform velocity. As expected, the refraction effect is greatest for small ray elevation angles.

The second invariant (Eq. (14)) is modified only slightly because each reflection point is generally at a different depth so that the elevation angle is altered by refraction. Incorporating Snell's law in the derivation of Eq. (14), we have for a trough of arbitrary cross section

$$\cos \theta_n \sin \phi_n / c_n = \cos \theta_0 \sin \phi_0 / c_0. \tag{56}$$

This equation was first derived by Weston [2]. Similarly, for a basin with rotational symmetry

$$\frac{r_n}{c_n} \cos \theta_n \sin \phi_n = \frac{r_0}{c_0} \cos \theta_0 \sin \phi_0. \tag{57}$$

Clearly, analytical ray paths cannot easily be obtained using Eqs. (54) and (56) or Eq. (57), but numerical solutions are possible.

V. SOUND INTENSITY IN TROUGHS AND BASINS

The spreading loss at a remote receiver may be calculated numerically by finding the final spacing in three dimensions of initially adjacent rays as given in sections II and III. This approach, however, does not throw much light on the relative importance of loss mechanisms such as geometric spreading and reflection or scattering loss.

A simpler way to look at the problem of propagation loss in a basin is to imagine (SOFAR) rays traveling across the center of the basin at constant azimuth because of the lack of bottom interaction, then curving round in a hyperbola on meeting a locally sloping plane bottom at the edge of the basin and then continuing as a SOFAR ray at a new heading. If we take the wedge model of Section II (ignoring the velocity structure near the edge of the basin), we see that the asymptotes of the hyperbola intersect at the zero depth contour (or the extrapolation to zero depth from the relevant part of the bottom if the bottom slope is not truly constant), so the horizontal projection consists, to a good approximation, of straight lines reflecting in the horizontal plane from the zero depth contours with each corner rounded off, as in Fig. 8, by a hyperbola.

Figure 9 shows the projection of two slightly diverging sets of SOFAR rays arriving at the base of the wedge and curving round in almost identical hyperbolic paths so that the resulting two sets of SOFAR rays are divergent by the same amount as before. By the invariants derived above the ray elevation angles for the incoming SOFAR rays on the left are the same as for the outgoing rays on the right. Thus, if the total time spent in the wedge region is small compared with that spent in the SOFAR region, the part of the loss associated with geometrical spreading is the same as if the SOFAR ray had carried on without any bottom interaction for the same total ray length. In other words, the intensity is proportional to $1/r$ where r is the total horizontal length of the ray. (It is assumed that ranges are large enough for the effects of convergence zones to have smoothed out.)

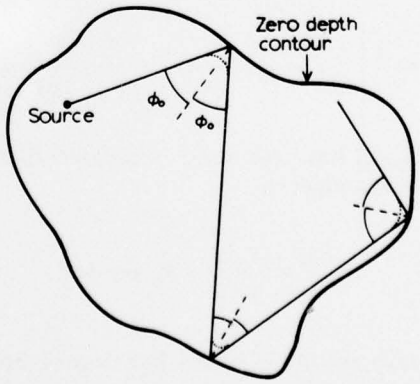

Fig. 8 — Method of constructing the horizontal projection of SOFAR rays after their hitting the basin edge

In practice, of course, the reflecting surface may differ from a simple tilted plane, but at the edge of a basin the greater part of the loss would probably come from the individual bottom reflections so the detailed geometrical effects may not be so important.

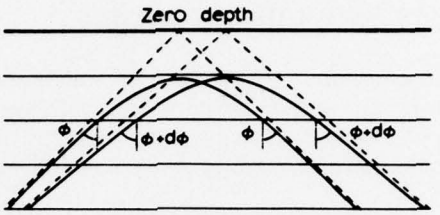

Fig. 9 — The horizontal divergence $d\phi$ of two sets of SOFAR rays is practically unchanged after encountering a straight basin edge

The number of bottom reflections encountered near the edge of a trough is given generally by

$$N = \int \frac{\sin\theta \, ds}{2H} = \frac{H_0 \sin\theta_0}{2 \sin\phi_0 \cos\theta_0} \int \frac{\tan\phi \, dy}{H^2} \, . \tag{58}$$

For a wedge of slope γ,

$$N = \frac{H_0}{\gamma^2} \int_{y_0}^{y_m} \frac{dy}{y[(\mathrm{cosec}^2\,\theta_0 - \cot^2\theta_0 \sin^2\phi_0)y^2 - y_0^2]^{1/2}} \, , \tag{59}$$

where the minimum y coordinate y_m of the hyperbola is

$$y_m = y_0 \sin\theta_0/(1 - \cos^2\theta_0 \sin^2\phi_0)^{1/2}.$$

The solution of the integral is

$$N = \frac{1}{\gamma}\left[\frac{\pi}{2} - \sin^{-1}\left(\frac{\sin\theta_0}{(1 - \cos^2\theta_0 \sin^2\phi_0)^{1/2}}\right)\right] \tag{60}$$

where the fact that $\gamma = H_0/y_0$ has been used. Provided that θ_0 is small and ϕ_0 is not too close to $\pi/2$, this may be expanded as

$$N = \frac{1}{\gamma}\left(\frac{\pi}{2} - \theta_0 \sec\phi_0\right). \tag{61}$$

Since most SOFAR rays are likely to hit the sloping bottom when they are at the lowest point of their trajectory, their initial ray angles for the above calculation are likely to be close to zero despite the fact that the initial angles for the SOFAR rays were arbitrary. The order of magnitude of loss L after an encounter with the edge of the basin is given in terms of R, the loss per bottom reflection (a logarithmic quantity) by

$$L = NR = \frac{\pi}{2\gamma} R.$$

R is in reality different for each reflection since it is a function of elevation angle; however, let us assume the worst case (the steepest angle) where, since at this point (the closest approach to shallow water) $\sin \phi = 1$, $\cos \theta_m = \cos \theta_0 \sin \phi_0$. As we have already assumed θ_0 to be small, we have $\theta_m \approx \pi/2 - \phi_0$.

Thus, the appropriate grazing angle in the vertical plane for evaluation of the reflection coefficient is simply the horizontal grazing angle to the edge of the basin (Fig. 8)

$$R = R(\theta) \approx R(\pi/2 - \phi_0). \tag{63}$$

The total loss on encountering the basin edge may be thought of as *the loss given by a single specular reflection at a vertical surface along the zero depth contour* made of the same material as the bottom multiplied by the real number of reflections* (which is roughly $\pi/2$ divided by the bottom slope). This is, of course, equivalent to the empirical scattering cross section already mentioned. The same interpretation serves as a quick method of constructing horizontal ray paths, and it may be shown by use of Eq. (24) that ray lengths are correct as well.

As an example, the reflection loss per bounce near the edge of the basin with $\phi_0 = 70^\circ$ as in Fig. 8 (and consequently $\theta_m = 20^\circ$) could be 1 dB with the 20° grazing angle and, say, a source frequency of 10 Hz. A bottom slope of 2° would give 45 bottom reflections and an overall reflection loss of 45 dB. The only other loss is that due to the usual spreading law for a source and receiver spaced apart by the total real ray length.

If, instead of the tilted-plane reflecting surface, a surface with gently curving depth contours such as a seamount had been chosen, the main difference in the above calculations would have been in the horizontal divergence of outgoing rays. From simple two-dimensional geometry it can be shown that the intensity vs range relation is now

$$I \propto \frac{u}{r_1(r_2 + u)}, \tag{64}$$

where

$$u = \frac{r_1 \rho \cos \Phi}{\rho \cos \Phi - 2r_1}, \tag{65}$$

where r_1, r_2, and ρ are source-seamount and seamount-receiver ranges and seamount radius of curvature, respectively, and 2Φ is the overall change in bearing of the ray. As expected, this makes the intensity inversely proportional to the total range $(r_1 + r_2)$ as the seamount radius of curvature tends to infinity, and, as the curvature becomes small compared with r_1 or r_2, the intensity is proportional to $(\rho/2) \cos \Phi/(r_1 r_2)$ which is equivalent to Weston's target strength formula.

---

*In the more general case of a bottom with unequally spaced contours, this would have to be the zero depth contour at the tangent plane to the bottom at, say, the closest approach to shallow water.

VI. CONCLUSION

Ray invariants were derived and used to calculate analytically the horizontal projection of surface- and bottom-reflected ray paths in the vicinity of submarine troughs, ridges, basins, and seamounts of various cross sections. The types of trajectories derived include a sine wave in a trough, a hyperbolic sine and hyperbolic cosine at a ridge, a hyperbola at a wedge, an ellipse in a circular basin, and a hyperbola-like curve at a conical seamount.

The ray length in a trough of constant cross section was found always to be proportional to the component of distance traveled along the trough, and, in a basin with rotational symmetry, the ray length was proportional to the area swept out by the radial coordinate of the ray.

Refraction was found not to affect greatly the horizontal projection of the ray path, although it makes solution in terms of simple functions impossible.

The reflection loss and geometrical spreading at the edge of a basin behave as if there had been a vertical reflecting surface at the zero-depth contour (see footnote, p. 19), with reflection coefficient identical to that of the real bottom except for being raised to the power $\pi/(2 \text{ bottom slope})$.

Many authors have adequately modeled echoes from seamounts and basin edges with an empirical scattering cross section or target strength for each feature. Some authors include a detailed single-scattering calculation [6]; others make no attempt to explain the target strength in detail and only imply a scattering (as opposed to reflection) model [7-9]. Only very rarely are the data entirely incompatible with the type of multiply-reflected ray paths investigated in this report, and in most cases these ray paths would probably fit the data more closely. In practice, determination of the correct mechanism by measuring the propagation loss is likely to be hampered by poor knowledge of environmental data, such as bottom roughness and reflection coefficient. Despite this, an experiment could be designed specifically to distinguish between the two mechanisms by measuring different variables such as transmission angle and arrival angle in the horizontal plane.

ACKNOWLEDGMENT

I should like to thank my hosts at NRL for bringing the problem to my attention and Dr. R. DeWitt for many useful discussions.

REFERENCES

1. D. E. Weston, "Guided Propagation in a Slowly Varying Medium," *Proc. Phys. Soc. Lond.* 73, 365-384 (1959).
2. D. E. Weston, "Horizontal Refraction in a Three-dimensional Medium of Variable Stratification," *Proc. Phys. Soc. Lond.* 78, 46-52 (1961).

3. D. M. Milder, "Ray and Wave Invariants for SOFAR Channel Propagation," *J. Acoust. Soc. Amer.* 46, 1259-1263 (1969).

4. I. M. Blatstein, "Ocean Basin Reverberation from Large Underwater Explosions Part I: Source Level and Propagation Loss Modelling," *SACLANTCEN Conf. Proc.* No. 17, Part 5, pp. 24-1, 24-9 (1975).

5. J. A. Goertner, Ocean Basin Reverberation from Large Underwater Explosions Part II: Computer Model for Reverberation, *SACLANTCEN Conf. Proc.* No. 17, Part 5, pp. 25-1, 25-14 (1975).

6. B. B. Adams, D. T. Deihl, L. B. Palmer, and J. T. Warfield, "Long-range Monostatic Reverberation in the Deep Ocean," *U.S. J. Underwater Acoust.* 24, 215-242 (Confidential Article, Unclassified Title) (1974).

7. J. Northrop, "Submarine Topographic Echoes from CHASE V," *J. Geophys. Res.* 73, 3909-3916 (1968).

8. A. C. Kibblewhite and R. N. Denham, "The CHASE V Explosion—Submarine Topographic Reflections from the Vicinity of Pitcairn Island," *Deep Sea Res.* 18, 905-911 (1971).

9. A. C. Kibblewhite and R. N. Denham, "Hydroacoustic Signals from the CHASE V Explosion," *J. Acoust. Soc. Amer.* 45, 944-956 (1969).

10. J. T. Warfield and J. M. Griffin, "Bistatic Seamount Reverberation in Active Surveillance," to be published in U.S. J. Underwater Acoust., Vol. 27, No. 4 (Confidential Article, Unclassified Title) (1977).